8

Particle production in high energy QCD

We now turn to the question of particle production in the saturation framework. We will work out explicitly the case of inclusive gluon production in high energy collisions. Again the calculation follows the two-step formalism we have seen before: we first find the gluon production in the quasi-classical approximation and then include quantum small-x evolution effects in the result. The methods that we present can be applied to the calculation of other particle production observables as well.

8.1 Gluon production at the lowest order

Consider gluon production in onium–onium collisions, studied in Chapter 3. The lowest-order gluon production takes place at order α_s^3 in the amplitude squared (order g^3 in the amplitude). The corresponding Feynman diagrams for high energy gluon production in quark–quark scattering are shown on the right-hand side of the equation in Fig. 3.6: in the case of onium–onium scattering one should also include a contribution where the antiquark line replaces either one or both quark lines. For quark–quark scattering the gluon production cross section can be obtained from Eq. (3.39): noticing that $dy = dk^+/k^+$ we write for the differential cross section

$$\frac{d\sigma}{d^2k_T dy} = \frac{2\alpha_s^3 C_F}{\pi^2}\frac{1}{k_T^2}\int d^2q_\perp \frac{1}{q_\perp^2(\vec{k}_\perp - \vec{q}_\perp)^2}. \tag{8.1}$$

Using the lowest-order unintegrated gluon distribution of a quark (cf. Eqs. (4.26) and (5.55)),

$$\phi_{LO}(k_T^2) = \frac{\alpha_s C_F}{\pi}\frac{1}{k_T^2}, \tag{8.2}$$

one can rewrite Eq. (8.1) in the following form:

$$\frac{d\sigma}{d^2k_T dy} = \frac{2\alpha_s}{C_F}\frac{1}{k_T^2}\int d^2q_\perp \phi_{LO}(q_T^2)\,\phi_{LO}\Big((\vec{k}_\perp - \vec{q}_\perp)^2\Big). \tag{8.3}$$

We see that the gluon production cross section consists of factorized contributions of the unintegrated gluon distributions ϕ_{LO} for each quark, convoluted with a q_T-integral (Gribov, Levin, and Ryskin 1983, Catani, Ciafaloni, and Hautmann 1991, Collins and Ellis 1991).

https://doi.org/10.1017/9781009291446.009 Published online by Cambridge University Press

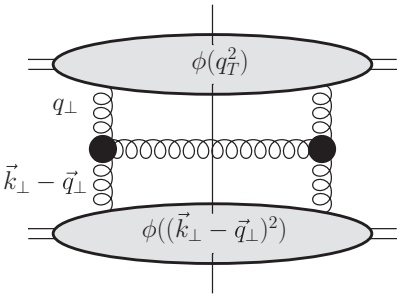

Fig. 8.1. Diagrammatic representation of k_T-factorization in Eq. (8.3). The vertical solid straight line denotes the final-state cut.

Such a factorization containing an integral over transverse momenta is known as a k_T-factorization as opposed to the more standard collinear factorization in perturbative QCD, in which there is no transverse momentum integral (Collins, Soper, and Sterman 1985a, b, 1988a, b).[1]

To obtain the gluon production cross section at order α_s^3 in the case of onium–onium scattering one has to sum over all possible diagrams of the type shown in Fig. 3.6, including the antiquark contributions both in the amplitude and in the complex conjugate amplitude (cf. Fig. 3.7). Eventually we see that Eq. (8.3) remains the answer for gluon production in the case of onium–onium scattering also, but with the unintegrated gluon distribution of an onium given by Eq. (3.92) instead of Eq. (8.2) and with the Green function G given by Eq. (3.59), so that

$$\phi_{LO}^{onium}(k_T^2) = \frac{\alpha_s C_F}{\pi} \frac{1}{k_T^2} \int d^2x_\perp \int_0^1 dz \, |\Psi(\vec{x}_\perp, z)|^2 \left(2 - e^{-i\vec{k}_\perp \cdot \vec{x}_\perp} - e^{i\vec{k}_\perp \cdot \vec{x}_\perp}\right), \tag{8.4}$$

where $\Psi(\vec{x}_\perp, z)$ is the bare onium wave function.

Equation (8.3) is illustrated in Fig. 8.1, where the shaded ovals denote the unintegrated distributions of the two onia and the solid circles denote Lipatov vertices. We see that, at this lowest order, the gluon production is given by factorized diagrams like that shown in Fig. 8.1, leading to the k_T-factorization expression (8.3).

Equation (8.1) can be integrated over $\vec{q}_\perp$ explicitly, with the help of the integral performed in appendix section A.3. This yields (cf. Gunion and Bertsch 1982)[2]

$$\frac{d\sigma}{d^2k_T dy} = \frac{8\alpha_s^3 C_F}{\pi} \frac{1}{k_T^4} \ln \frac{k_T}{\Lambda}, \tag{8.5}$$

with Λ an IR cutoff as usual. There is a problem with Eq. (8.5): if we integrate both sides over $\vec{k}_\perp$ to obtain the integrated cross section $d\sigma/dy$ we would get $d\sigma/dy \sim (1/\Lambda^2) \ln \Lambda$.

[1] A proper discussion of particle production in the collinear factorization framework is beyond the scope of this book. Instead we refer the reader to the textbook by Sterman (1993) and the monograph by Collins (2011) and the references therein.

[2] In the framework of the MV model, Eq. (8.5) was derived by Kovner, McLerran, and Weigert (1995a, b) and by Kovchegov and Rischke (1997).

https://doi.org/10.1017/9781009291446.009 Published online by Cambridge University Press

Thus the integrated cross section depends on the nonperturbative IR cutoff in a power-law way, indicating that one probably should not calculate $d\sigma/dy$ using a perturbative approach.

A similar problem remains for the net gluon multiplicity, which is defined by

$$\frac{dN}{d^2k_T dy} = \frac{1}{\sigma_{inel}} \frac{d\sigma}{d^2k_T dy} \tag{8.6}$$

with σ_{inel} the total inelastic scattering cross section. At the lowest-order, two-gluon-exchange, level, we have $\sigma_{inel} \sim 1/\Lambda^2$. Combining this with $d\sigma/dy \sim (1/\Lambda^2)\ln\Lambda$ we see that the gluon–gluon multiplicity scales as $dN/dy \sim \ln\Lambda$, i.e., it is also IR-cutoff-dependent, though the dependence is logarithmic and so is much softer than that for $d\sigma/dy$.

These IR problems in $d\sigma/dy$ and dN/dy are remedied by saturation physics, which again enables the use of the perturbative approximation. Above we have seen several examples of how saturation effects screen the IR region, making observables much less dependent on nonperturbative physics; we will now see how this happens for the inclusive gluon production.

8.2 Gluon production in DIS and pA collisions

8.2.1 Quasi-classical gluon production

Let us now try to generalize the leading-order gluon production cross section we have just obtained to the case of gluon production in DIS on a nucleus. Our observable is the single-particle inclusive gluon production: we want to measure a gluon in the final state without any constraints on what else can be present in the final state. (Because of the lack of final-state constraints this observable is referred to as "inclusive", as opposed to exclusive processes such as diffraction.) We will be working in the quasi-classical MV/GGM approximation. Just as for the total DIS cross section we can factor out the light cone wave function for a virtual photon splitting into a $q\bar{q}$ pair and consider only the dipole–nucleus scattering. According to the MV model, the gluon production in DIS should be obtained by finding the classical gluon field solution of the Yang–Mills equations (5.4) with the source current now given by the nucleus and the $q\bar{q}$ dipole. One may also consider gluon production in proton–nucleus (pA) collisions: in this case the source current is given by the nucleus and the proton. The difference between a nucleus and a proton in the saturation picture is that the proton's saturation scale Q_{s1} is much smaller than the nuclear saturation scale Q_{s2}, i.e., $Q_{s1} \ll Q_{s2}$. Therefore, when one is considering gluon production with transverse momentum $k_T \gg Q_{s1}$ and making no assumption about the relation between k_T and Q_{s2}, one can neglect multiple interactions with the proton and other saturation effects in the proton wave function while keeping multiple rescatterings to all orders in the nucleus. As we saw in Chapter 5 the classical MV treatment resums the parameter $\alpha_s^2 A^{1/3}$ resulting from two-gluon exchanges with each nucleon and in this way is equivalent to the GGM approach. We conclude that, working either in the light cone gauge of the dipole (proton),

https://doi.org/10.1017/9781009291446.009 Published online by Cambridge University Press

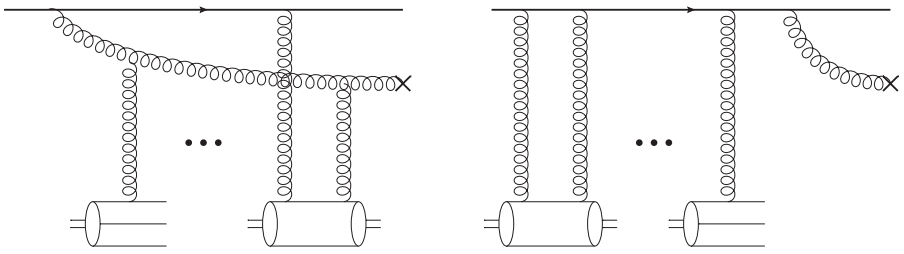

Fig. 8.2. Diagrams contributing to the gluon production amplitude in quark–nucleus collisions. The cross denotes the measured gluon.

or in the covariant gauge, when resumming the diagrams for gluon production we have to include all the multiple two-gluon rescatterings on the nucleons in the nucleus.

For simplicity we begin by calculating gluon production in quark–nucleus scattering. We work in a frame in which the nucleus is moving along the x^+-direction while the quark is moving along the x^--direction. The calculation is simpler in the $A^- = 0$ gauge, which we will be using. This gauge is equivalent to the $\partial_\mu A^\mu = 0$ covariant gauge for the nucleus. The LCPT diagrams contributing to gluon production in quark–nucleus collisions in the $A^- = 0$ gauge are shown in Fig. 8.2. Analogously to the case of small-x evolution considered above, the gluon's minus component of momentum is much smaller than that of the incoming quark. Gluon emission may take place either before or after the interaction with the target (cf. Fig. 4.24 and the accompanying explanation of why emissions during the interaction are suppressed by a power of s). Interactions with the nucleons in the target may be both elastic and inelastic.

Just as before, calculation of the diagrams is easier to carry out in transverse coordinate space. However, in the end we need to find the differential production cross section in momentum space. To connect the momentum-space cross section to transverse coordinate space let us go back to the lowest-order gluon production from the previous section. The lowest-order term in Eq. (8.1) is given by (see Sec. 3.3.1)

$$\frac{d\sigma}{d^2k_T dy} = \frac{1}{2(2\pi)^3}\int \frac{d^2q}{(2\pi)^2}\frac{1}{4s^2}\langle |M_{qq\to qqG}(\vec{k}_\perp, \vec{q}_\perp)|^2\rangle \tag{8.7}$$

where the scattering amplitude $M_{qq\to qqG}$ is given in Eq. (3.35) and s is the center-of-mass energy squared of the collision. Defining a rescaled amplitude by (cf. Eq. (B.22))

$$A(\vec{k}_\perp, \vec{q}_\perp) = \frac{M_{qq\to qqG}(\vec{k}_\perp, \vec{q}_\perp)}{2s}, \tag{8.8}$$

we can rewrite Eq. (8.7) as

$$\frac{d\sigma}{d^2k_T dy} = \frac{1}{2(2\pi)^3}\int \frac{d^2q}{(2\pi)^2}\langle |A(\vec{k}_\perp, \vec{q}_\perp)|^2\rangle. \tag{8.9}$$

https://doi.org/10.1017/9781009291446.009 Published online by Cambridge University Press

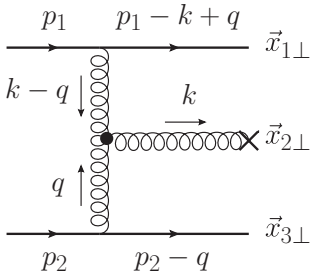

Fig. 8.3. Gluon production at the lowest order with the transverse coordinates shown explicitly.

To Fourier-transform the amplitude $A(\vec{k}_\perp, \vec{q}_\perp)$ into transverse coordinate space we use

$$A(\vec{x}_{23}, \vec{x}_{13}) = \int \frac{d^2k_\perp}{(2\pi)^2} \frac{d^2q_\perp}{(2\pi)^2} e^{i\vec{k}_\perp \cdot \vec{x}_{21} + i\vec{q}_\perp \cdot \vec{x}_{13}} A(\vec{k}_\perp, \vec{q}_\perp), \tag{8.10}$$

where as usual $\vec{x}_{ij} = \vec{x}_{i\perp} - \vec{x}_{j\perp}$. Equation (8.10) is illustrated in Fig. 8.3 for one of the lowest-order diagrams from Fig. 3.6. Remember that in eikonal interactions the transverse coordinates of the particles remain unchanged: hence the colliding quarks have transverse coordinates $\vec{x}_{1\perp}$ and $\vec{x}_{3\perp}$ both before and after the interaction. Also note that the amplitude $M_{qq\to qqG}$ and with it $A(\vec{k}_\perp, \vec{q}_\perp)$ already have momentum conservation imposed on them: this leads to translational invariance in coordinate space, making the coordinate-space amplitude $A(\vec{x}_{23}, \vec{x}_{13})$ in Eq. (8.10) a function of the differences between the transverse vectors only.

Inverting Eq. (8.10) we get

$$A(\vec{k}_\perp, \vec{q}_\perp) = \int d^2x_2 d^2x_0 e^{-i\vec{x}_{2\perp}\cdot\vec{k}_\perp - i\vec{x}_{1\perp}\cdot(\vec{q}_\perp - \vec{k}_\perp)} A(\vec{x}_{23}, \vec{x}_{13}). \tag{8.11}$$

Using this in Eq. (8.9) and integrating over $\vec{q}_\perp$ we obtain

$$\frac{d\sigma}{d^2k_T dy} = \frac{1}{2(2\pi)^3} \int d^2x_2 d^2x_{2'} d^2x_1 e^{-i\vec{k}_\perp \cdot \vec{x}_{22'}} \langle A(\vec{x}_{23}, \vec{x}_{13}) A^*(\vec{x}_{2'3}, \vec{x}_{13}) \rangle, \tag{8.12}$$

where $\vec{x}_{2\perp}$ and $\vec{x}_{2'\perp}$ are the transverse coordinates of the gluon in the amplitude and in the complex conjugate amplitude respectively. We see that the reason that the two coordinates are different is that we are keeping the transverse momentum of the gluon $\vec{k}_\perp$ fixed: if we integrated Eq. (8.12) over $\vec{k}_\perp$ this would make $\vec{x}_{2\perp}$ and $\vec{x}_{2'\perp}$ equal. One can think of the difference between $\vec{x}_{2\perp}$ and $\vec{x}_{2'\perp}$ as due to the uncertainty principle: if we know the momentum $\vec{k}_\perp$ exactly, we cannot have precise knowledge of the transverse position of the gluon. Note that since we do not keep the transverse momenta of the two quarks in the final state fixed and, rather, allow them to be arbitrary (that is, we integrate over all their values), the transverse coordinates of the quarks are the same in the amplitude and in the complex conjugate amplitude.

https://doi.org/10.1017/9781009291446.009 Published online by Cambridge University Press

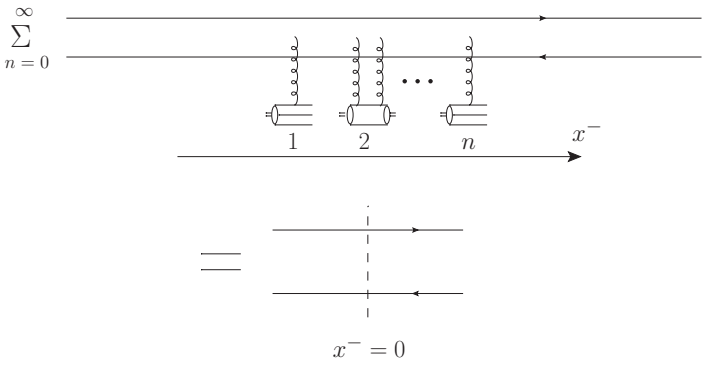

Fig. 8.4. An extension of the notation of Fig. 5.8 to include inelastic interactions between the projectile and the nucleons in the target nucleus.

Note that for a nuclear target with the quark at $\vec{x}_{3\perp}$ part of a nucleon in the nucleus, the angle brackets in Eq. (8.12) would imply an average over all positions of the nucleon,

$$\int d^2x_3 T(\vec{x}_{3\perp}), \tag{8.13}$$

where $T(\vec{x}_{3\perp})$ is the nuclear profile function defined in Eq. (4.31).

Equation (8.12), while derived for the lowest-order gluon production, is applicable for gluon production in any process involving the eikonal scattering of a quark (or any other projectile, such as an onium or a proton) on a target nucleus, including multiple rescatterings and small-x evolution. In deriving Eq. (8.12) we had to rescale the scattering amplitude in Eq. (8.8): however, it is possible to see that in the GGM multiple rescattering case each additional nucleon enters with the same normalization factor, so that the net scattering amplitude (4.51) is energy independent. In addition, in eikonal scattering and LLA small-x evolution the transverse coordinates of the gluons and quarks do not change, which implies that the transverse vectors $\vec{x}_{2\perp}$, $\vec{x}_{2'\perp}$, and $\vec{x}_{1\perp}$ in Eq. (8.12) will not change if we allow the quark and the gluon to multiply rescatter and branch out into more gluons in the LLA approximation. We conclude that Eq. (8.12) is the required relation between the momentum-space cross section and the coordinate-space scattering amplitude.

Squares of the diagrams in Fig. 8.2 giving the production cross section are shown in Fig. 8.5 using the slight extension defined in Fig. 8.4 of the notation from Fig. 5.8 for the interaction of the projectile with the target: now the vertical dashed line includes both elastic and inelastic interactions with the target. Beyond the diagrams, the notation in Fig. 5.8 includes the averaging of Wilson lines over the target fields while the notation of Fig. 8.4 does not. The graphs shown in Fig. 8.5 represent the amplitude squared, with two time axes, one in the amplitude and one in the complex conjugate amplitude, just as in the case of diffraction considered above.

Figure 8.5 demonstrates all the main cases one has to consider. If x^-_{em} is the light cone time of the gluon emission in the amplitude while x'^-_{em} is that in the complex conjugate amplitude (see diagram C in Fig. 8.5), we have four cases represented in Fig. 8.5, as follows.

https://doi.org/10.1017/9781009291446.009 Published online by Cambridge University Press

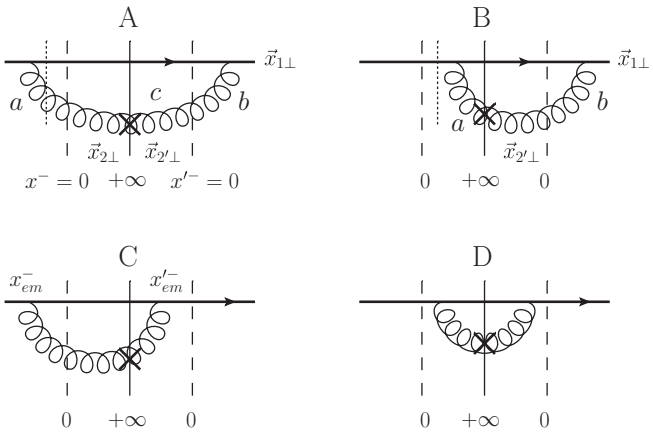

Fig. 8.5. Diagrams contributing to gluon production in quark–nucleus collisions. The cross denotes the measured gluon.

(A) $x^-_{em} < 0$, $x'^-_{em} < 0$: the gluon is emitted before the interaction with the target both in the amplitude and in the complex conjugate amplitude.
(B) $x^-_{em} > 0$, $x'^-_{em} < 0$: the gluon is emitted after the interaction with the target in the amplitude but before the interaction with the target in the complex conjugate amplitude.
(C) $x^-_{em} < 0$, $x'^-_{em} > 0$: the gluon is emitted before the interaction with the target in the amplitude but after the interaction with the target in the complex conjugate amplitude.
(D) $x^-_{em} > 0$, $x'^-_{em} > 0$: the gluon is emitted after the interaction with the target both in the amplitude and in the complex conjugate amplitude.

We need to find the amplitude squared in transverse coordinate space to use in Eq. (8.12). To do this we have to calculate the diagrams in Fig. 8.5. The transverse coordinates of the quark ($\vec{x}_{1\perp}$) together with the coordinates $\vec{x}_{2\perp}$ and $\vec{x}_{2'\perp}$ of the gluon to the left and to the right of the final state cut are shown in panel A of Fig. 8.5. The calculation is easier to carry out using LCPT, in which the process factorizes into the light cone wave function for a quark splitting into a quark and a gluon and the amplitude for the interaction with the target.

The soft gluon emission brings in a factor (cf. Eq. (4.60))

$$i\frac{gt^a}{\pi}\frac{\vec{\epsilon}^{\lambda *}_{\perp}\cdot\vec{x}_{21}}{x^2_{21}} \tag{8.14}$$

in the amplitude and the same (but conjugate) factor with the index 2 replaced by $2'$ in the complex conjugate amplitude, along with $a \to b$ (the gluon colors allocation is given in Fig. 8.5A). In Eq. (8.14), λ is the polarization of the gluon, which remains unchanged in the eikonal interaction with the target and is therefore the same on both sides of the cut. Emissions with either $x^-_{em} > 0$ or $x'^-_{em} > 0$ lead to an extra minus sign compared with the early-time emissions: this can be deduced from panels A and B of Fig. 8.5. There the vertical

https://doi.org/10.1017/9781009291446.009 Published online by Cambridge University Press

dashed lines denote the intermediate states in the amplitudes A and B used in calculating the quark splitting corresponding to Eq. (8.14). In panel B the intermediate state contains only a quark (with the rest of the target, not shown): in building up the energy denominator for this state we have to take the light cone energy of the quark (and the outgoing target) and subtract the light cone energy of the incoming state, or, equivalently, the energy of the outgoing state. We thus obtain the light cone energy of the intermediate-state quark minus the energies of the outgoing quark and gluon. This is the negative of the energy denominator for the intermediate state highlighted by the dotted line in panel A of Fig. 8.5. We see that the late-time emissions bring in an extra minus sign. This conclusion is similar to that regarding the sign difference used in deriving the cancellations in panel B of Fig. 7.10 (see Eqs. (7.34) and (7.35)). To summarize, diagrams B and C in Fig. 8.5 have an extra minus sign compared with diagrams A and D in the same figure.

We now need to calculate the interactions with the target in each panel of Fig. 8.5. This is easiest to do using the language of Wilson lines defined in Eqs. (5.43) and (5.44). The interaction with the target in Fig. 8.5A (along with the color factors resulting from the gluon emission) gives

$$\left\langle \frac{1}{N_c}\mathrm{tr}\left[t^b V^\dagger_{\vec{x}_{1\perp}} V_{\vec{x}_{1\perp}} t^a\right] U^{bc}_{\vec{x}_{2'\perp}} U^{ca}_{\vec{x}_{2\perp}} \right\rangle = C_F S_G(\vec{x}_{2\perp}, \vec{x}_{2'\perp}, y), \tag{8.15}$$

where we have used Eq. (5.33) and definition (5.46) to simplify the expression. As in the case of the calculation in Sec. 3.3.1 we assume that the target nucleus has rapidity 0 while the produced gluon along with the quark that emits it have rapidity y. Note that the quark's interaction with the target cancels out in diagram A: the quark becomes a "spectator" and the interaction is given by the gluon dipole S-matrix.

The contribution of Fig. 8.5B is obtained similarly, yielding, with the help of Eq. (5.31),

$$\left\langle \frac{1}{N_c}\mathrm{tr}\left[t^a V^\dagger_{\vec{x}_{1\perp}} t^b V_{\vec{x}_{1\perp}}\right] U^{ba}_{\vec{x}_{2'\perp}} \right\rangle = C_F S_G(\vec{x}_{1\perp}, \vec{x}_{2'\perp}, y). \tag{8.16}$$

By analogy diagram C brings in

$$C_F S_G(\vec{x}_{2\perp}, \vec{x}_{1\perp}, y) \tag{8.17}$$

and diagram D contributes only a factor C_F.

Combining the emission contribution (8.14) with the interaction terms we have just found, and using it all in Eq. (8.12) while keeping in mind that diagrams B and C have an extra minus sign, we obtain, after summation over the gluon polarizations (Kovchegov and Mueller 1998a):

$$\frac{d\sigma^{qA}}{d^2k_T dy} = \frac{1}{(2\pi)^2}\int d^2x_2\, d^2x_{2'}\, d^2x_1 e^{-i\vec{k}_\perp\cdot\vec{x}_{22'}} \frac{\alpha_s C_F}{\pi^2}\frac{\vec{x}_{21}\cdot\vec{x}_{2'1}}{x_{21}^2 x_{2'1}^2}$$
$$\times\left[S_G(\vec{x}_{2\perp}, \vec{x}_{2'\perp}, y) - S_G(\vec{x}_{1\perp}, \vec{x}_{2'\perp}, y) - S_G(\vec{x}_{2\perp}, \vec{x}_{1\perp}, y) + 1\right]. \tag{8.18}$$

This result was independently confirmed by Kopeliovich, Tarasov, and Schafer (1999) and by Dumitru and McLerran (2002). Equation (8.18) can also be rewritten in terms of the

https://doi.org/10.1017/9781009291446.009 Published online by Cambridge University Press

imaginary part of the gluon dipole–nucleus forward scattering amplitude,

$$N_G(\vec{x}_{1\perp}, \vec{x}_{0\perp}, Y) = 1 - S_G(\vec{x}_{1\perp}, \vec{x}_{0\perp}, Y), \tag{8.19}$$

as follows:

$$\frac{d\sigma^{qA}}{d^2k_T dy} = \frac{1}{(2\pi)^2} \int d^2x_2\, d^2x_{2'}\, d^2x_1 e^{-i\vec{k}_\perp \cdot \vec{x}_{22'}} \frac{\alpha_s C_F}{\pi^2} \frac{\vec{x}_{21} \cdot \vec{x}_{2'1}}{x_{21}^2 x_{2'1}^2} \times \left[N_G(\vec{x}_{1\perp}, \vec{x}_{2'\perp}, y) + N_G(\vec{x}_{2\perp}, \vec{x}_{1\perp}, y) - N_G(\vec{x}_{2\perp}, \vec{x}_{2'\perp}, y) \right]. \tag{8.20}$$

While our derivation of Eq. (8.20) was quite general, in the MV/GGM quasi-classical approximation one should use the amplitude N_G given by Eq. (5.51) in Eq. (8.20). In that approximation for N_G, Eq. (8.20) would give us the gluon production in quark–nucleus scattering in the quasi-classical MV/GGM approximation.

It is interesting to note that Eq. (8.20) can be rewritten in the k_T-factorized form seen in Eq. (8.3). To see this we integrate over $\vec{x}_{2\perp}$ in the first term in the square brackets of Eq. (8.20), over $\vec{x}_{2'\perp}$ in the second term in the same brackets, and over $\vec{x}_{1\perp}$ in the third term, with the help of Eqs. (A.10) and (A.12). This yields, after some coordinate relabeling,

$$\frac{d\sigma^{qA}}{d^2k_T dy} = \frac{\alpha_s C_F}{2\pi^3} \int d^2x_2\, d^2x_{2'} e^{-i\vec{k}_\perp \cdot \vec{x}_{22'}} \left(2i \frac{\vec{k}_\perp}{k_\perp^2} \cdot \frac{\vec{x}_{22'}}{x_{22'}^2} - \ln \frac{1}{x_{22'}\Lambda} \right) \times N_G(\vec{x}_{2\perp}, \vec{x}_{2'\perp}, y) \tag{8.21}$$

with Λ again an IR cutoff. Using the fact that $N_G(\vec{x}_{2\perp} = \vec{x}_{2'\perp}, \vec{x}_{2'\perp}, Y) = 0$ (a zero-size dipole does not interact), we can rewrite Eq. (8.21) as

$$\frac{d\sigma^{qA}}{d^2k_T dy} = \frac{\alpha_s C_F}{2\pi^3} \frac{1}{k_T^2} \int d^2x_2\, d^2x_{2'} N_G(\vec{x}_{2\perp}, \vec{x}_{2'\perp}, y) \nabla^2_{\vec{x}_{2\perp}} \left(e^{-i\vec{k}_\perp \cdot \vec{x}_{22'}} \ln \frac{1}{x_{22'}\Lambda} \right), \tag{8.22}$$

where $\nabla^2_{\vec{x}_\perp} = \partial^2_{x^1} + \partial^2_{x^2}$ is the two-dimensional Laplace operator.

Let us write Eq. (8.22) in a projectile–target-symmetric way. The expression already contains the dipole–nucleus scattering amplitude N_G. Let us include the dipole–projectile scattering amplitude in it as well. Since our projectile is a single quark, we will construct the scattering amplitude of a gluon dipole on a quark in the quasi-classical approximation by expanding Eq. (5.51) to the lowest nontrivial order and using $Q_{sG}^2(\vec{b}_\perp) = 4\pi\alpha_s^2 T_q(\vec{b}_\perp)$ with the "nuclear profile function" of a single quark, normalized such that

$$\int d^2b_\perp T_q(\vec{b}_\perp) = 1. \tag{8.23}$$

(The factor 2 difference between the value of Q_{sG}^2 that we are using now and that in Eq. (5.41) arises because the saturation scale in Eq. (5.41) is due to scattering on an onium "nucleon" while now we are dealing with a single-quark "nucleon".) We obtain for the dipole–quark scattering amplitude n_G^q at the two-gluon exchange level, integrated over all

https://doi.org/10.1017/9781009291446.009 Published online by Cambridge University Press

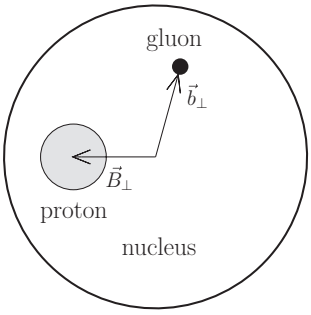

Fig. 8.6. Gluon production in proton(quark)–nucleus collisions as seen in the transverse plane. To make the figure clearer, the gluon has been placed far from the proton; this is, however, a highly improbable configuration.

impact parameters $\vec{b}_\perp$,

$$\int d^2b_\perp \, n_G^q(\vec{x}_\perp, \vec{b}_\perp, Y = 0) = \pi \alpha_s^2 x_\perp^2 \ln \frac{1}{x_\perp \Lambda}, \tag{8.24}$$

where $\vec{x}_\perp$ is the dipole's transverse size and $\vec{b}_\perp$ is the location of its center-of-mass.

Neglecting constants under the logarithms (which were neglected in arriving at Eq. (8.24) anyway), we write

$$\nabla^2_{\vec{x}_\perp} \left(x_\perp^2 \ln \frac{1}{x_\perp \Lambda} \right) = 4 \ln \frac{1}{x_\perp \Lambda}. \tag{8.25}$$

Using this formula together with Eq. (8.24) in Eq. (8.22) yields, after integration by parts in the latter,

$$\frac{d\sigma^{qA}}{d^2k_T dy} = \frac{C_F}{\alpha_s \pi (2\pi)^3} \frac{1}{k_T^2} \int d^2B_\perp d^2b_\perp d^2x_\perp \left[\nabla^2_{\vec{x}_\perp} n_G^q(\vec{x}_\perp, \vec{B}_\perp - \vec{b}_\perp, 0) \right] \times e^{-i\vec{k}_\perp \cdot \vec{x}_\perp} \left[\nabla^2_{\vec{x}_\perp} N_G(\vec{x}_\perp, \vec{b}_\perp, y) \right], \tag{8.26}$$

where $\vec{x}_\perp = \vec{x}_{22'}$ and we have modified the notation as follows:

$$N_G(\vec{x}_{2\perp}, \vec{x}_{2'\perp}, Y) \to N_G(\vec{x}_\perp, \vec{b}_\perp, Y). \tag{8.27}$$

Now $\vec{B}_\perp$ and $\vec{b}_\perp$ are the impact parameters of the proton and the produced gluon respectively, measured with respect to the center of the nucleus, as shown in Fig. 8.6.

Equation (8.26) describes gluon production in quark–nucleus scattering. However, it can be generalized to the onium–nucleus (DIS) and proton–nucleus (pA) cases if n_G^q in it is replaced by the dipole scattering amplitude on the onium (see Eq. (3.139)) or on a proton, labeled n_G. (The proton can be modeled as three valence quarks in a color-singlet state or as any other number of partons moving along the light cone.) Proving this statement for the onium–nucleus scattering is left as an exercise for the reader (see Exercise 8.2). We can conclude that Eq. (8.26) with N_G taken at $y = 0$ and n_G^q replaced by n_G describes

https://doi.org/10.1017/9781009291446.009 Published online by Cambridge University Press

quasi-classical gluon production in onium–nucleus (DIS) and pA collisions. We will refer to it as quasi-classical gluon production in the pA collision context.

Defining the unintegrated gluon distribution for the nucleus (in the quasi-classical MV/GGM approximation) as

$$\phi_A(k_T^2) = \frac{C_F}{\alpha_s (2\pi)^3} \int d^2 b_\perp d^2 x_\perp e^{-i\vec{k}_\perp \cdot \vec{x}_\perp} \nabla^2_{\vec{x}_\perp} N_G \left(\vec{x}_\perp, \vec{b}_\perp, 0 \right) \tag{8.28}$$

and that for the proton as

$$\phi_p(k_T^2) = \frac{C_F}{\alpha_s (2\pi)^3} \int d^2 b_\perp d^2 x_\perp e^{-i\vec{k}_\perp \cdot \vec{x}_\perp} \nabla^2_{\vec{x}_\perp} n_G(\vec{x}_\perp, \vec{b}_\perp, 0), \tag{8.29}$$

transforms Eq. (8.26) into a k_T-factorized form of Eq. (8.3) (Kovchegov and Tuchin 2002):

$$\frac{d\sigma^{pA}}{d^2 k_T \, dy} = \frac{2\alpha_s}{C_F} \frac{1}{k_T^2} \int d^2 q_\perp \, \phi_p(q_T^2) \, \phi_A \left((\vec{k}_\perp - \vec{q}_\perp)^2 \right), \tag{8.30}$$

where now we use the superscript pA to signify the broader validity range of the derived cross section. (Again we have put $y = 0$ in the argument of N_G in Eq. (8.28) to reduce Eq. (8.26) to the purely quasi-classical case.)

Equation (8.30) may come as a surprise: remember that k_T-factorization usually results from factorizing the diagrams into the form shown in Fig. 8.1, separating them into distribution functions with a Lipatov vertex (squared) in the middle. The diagrams in Fig. 8.5 which led to Eq. (8.30) have no such factorization, since they include direct interactions between the target nucleus and the projectile quark, violating the factorization picture expected from Fig. 8.1. One may hope that perhaps in a different gauge the relevant diagrams would factorize, yielding the picture of Fig. 8.1; to date, however, no such gauge has been found and the physical origin of the k_T-factorization in Eq. (8.30) remains a mystery.

Notice that to achieve the factorized expression (8.30) we had to define the unintegrated gluon distributions (8.28) and (8.29). These definitions are different from the WW distribution of Eq. (5.50) and are more in line with Eq. (6.16) with the quark dipole replaced by the gluon one. (All the distributions agree at the lowest order of Eq. (8.2) up to quark or gluon dipole color factors.) While the definitions (8.28) and (8.29) allow us to achieve the k_T-factorization formula (8.30), it is *a priori* not clear why one has to use these gluon distributions in the gluon production formula. The interplay between the two unintegrated gluon distributions has recently been explored by Dominguez *et al.* (2011).

To assess the impact of (8.30) on the k_T-distribution of the produced gluons (also known as the gluon transverse momentum spectrum) let us evaluate its large-k_T and small-k_T asymptotics. At large k_T we expand Eq. (5.51) to the lowest nontrivial order to get $N_G = x_\perp^2 Q_{sG}^2(\vec{b}_\perp)/4$, which we use in Eq. (8.28) to obtain the lowest-order ϕ_A. For simplicity, modeling the proton again as a single quark, we use Eq. (8.24) in Eq. (8.29) to obtain the same expression for ϕ_p as in (8.2). Finally, substituting all this into Eq. (8.30) and remembering that $Q_{sG}^2(\vec{b}_\perp) = 4\pi\alpha_s^2 T(\vec{b}_\perp)$, we obtain

$$\left. \frac{d\sigma^{pA}}{d^2 k_T \, dy} \right|_{k_T \gg Q_{sG}} \approx \frac{8\alpha_s^3 C_F A}{\pi} \frac{1}{k_T^4} \ln \frac{k_T}{\Lambda}, \tag{8.31}$$

https://doi.org/10.1017/9781009291446.009 Published online by Cambridge University Press

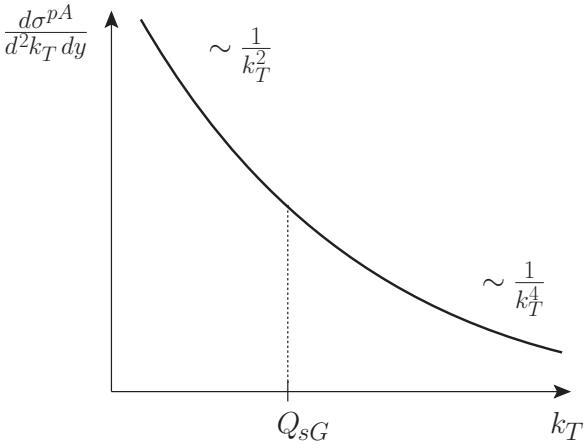

Fig. 8.7. A sketch of the gluon production spectrum generated by Eq. (8.30).

in agreement with Eq. (8.5) up to a factor A, signifying that now we have A nucleons in the nucleus that can interact with the incoming projectile quark to produce the gluon that we are measuring (again with each nucleon modeled by a single quark). Conversely, at $k_T \ll Q_{sG}$ we note that $N_G \approx 1$ for $x_\perp > 1/Q_{sG}$. Using this approximation in Eq. (8.21) and integrating over $\vec{x}_{2\perp}, \vec{x}_{2'\perp}$ yields

$$\left.\frac{d\sigma^{pA}}{d^2k_T\,dy}\right|_{k_T \ll Q_{sG}} \approx \frac{\alpha_s C_F S_\perp}{\pi^2}\frac{1}{k_T^2} \tag{8.32}$$

with $S_\perp$ the transverse area of the nucleus. We see that the produced gluon spectrum has been modified by saturation effects from the factor $1/k_T^4$ in Eq. (8.31) at $k_T \gg Q_{sG}$ to the factor $1/k_T^2$ in Eq. (8.32) at $k_T \ll Q_{sG}$. This is illustrated in Fig. 8.7 (cf. Fig. 5.7). We conclude that saturation effects in one scattering particle (the nucleus) tend to soften the IR divergence, making the integrated cross section dependent on the IR cutoff only logarithmically, $d\sigma^{pA}/dy \sim \ln(Q_{sG}/\Lambda)$.

To better understand the result (8.30) it is useful to construct the *nuclear modification factor*, which in pA collisions can be defined as

$$R^{pA}(k_T, y) = \frac{d\sigma^{pA}/d^2k_T\,dy}{A\,d\sigma^{pp}/d^2k_T\,dy}. \tag{8.33}$$

and has the meaning of the ratio of the number of particles produced in a pA collision per individual proton–nucleon collision and the number of particles produced in a proton–proton (pp) collision in the same kinematic region. Deviations of the nuclear modification factor from unity measure collective nuclear effects in the collision.

In the quasi-classical approximation one can evaluate R^{pA} by using N_G from Eq. (5.51) in Eq. (8.20) to find the gluon production in pA collisions and by using n_G^q from Eq. (8.24), instead of N_G, in the same formula to find the gluon production in pp. The resulting nuclear modification factor is plotted in Fig. 8.8 (Kopeliovich, Tarasov, and Schafer 1999, Baier,

https://doi.org/10.1017/9781009291446.009 Published online by Cambridge University Press

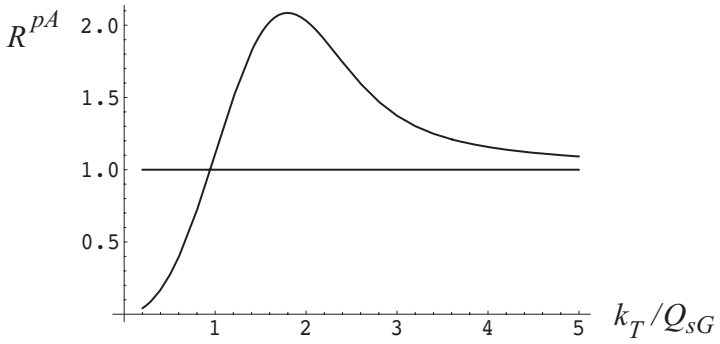

Fig. 8.8. Nuclear modification factor as a function of k_T/Q_{sG} for gluon production in pA collisions in the quasi-classical approximation. The horizontal line at $R^{pA} = 1$ is shown to guide the eye. Since Eq. (8.33) includes an integral over $b_\perp$, Q_{sG} should be understood as the typical saturation scale: the same Cronin enhancement is also seen for fixed $b_\perp$. (Reprinted with permission from Kharzeev, Kovchegov, and Tuchin (2003). Copyright 2003 by the American Physical Society.)

Kovner, and Wiedemann 2003, Kharzeev, Kovchegov, and Tuchin 2003): we see a depletion in the produced gluons at low k_T ($k_T \ll Q_{sG}$) and an enhancement at large k_T ($k_T \gtrsim Q_{sG}$). We conclude that multiple rescatterings tend to broaden the k_T-distribution of the produced gluons, effectively pushing the gluons out to large k_T. The enhancement shown in Fig. 8.8 was observed experimentally in hadron production in pA collisions and is known as the *Cronin effect* (Cronin *et al.* 1975).

The suppression of gluons at low k_T may be identified with the manifestation of nuclear shadowing in the saturation/CGC framework. In the case of gluons the shadowing is quantified by the ratio

$$R_A(x, Q^2) = \frac{xG_A(x, Q^2)}{AxG_N(x, Q^2)} \tag{8.34}$$

(with an analogous ratio for quarks). The shadowing ratio R_A measures the number of gluons per nucleon in the nucleus divided by the number of gluons in a proton (in the same kinematic region). At small x the ratio R_A is known to be below 1, which means that the number of gluons per nucleon in a nucleus is less than the number of gluons in a free proton: this effect is known as nuclear shadowing. (For more on nuclear shadowing see Frankfurt and Strikman (1988).) This depletion of gluons in the nuclear wave function leads to the suppression of produced gluons as measured by the nuclear modification factor. In fact, one can show that the suppression of produced gluons at low k_T in Fig. 8.8 results from the suppression of low-k_T gluons in the unintegrated gluon distribution of Eq. (8.28).

8.2.2 Including nonlinear evolution

We want to include the effects of nonlinear LLA small-x evolution in the inclusive gluon production cross section (8.20) and in the more general cross section (8.30). Again we

https://doi.org/10.1017/9781009291446.009 Published online by Cambridge University Press

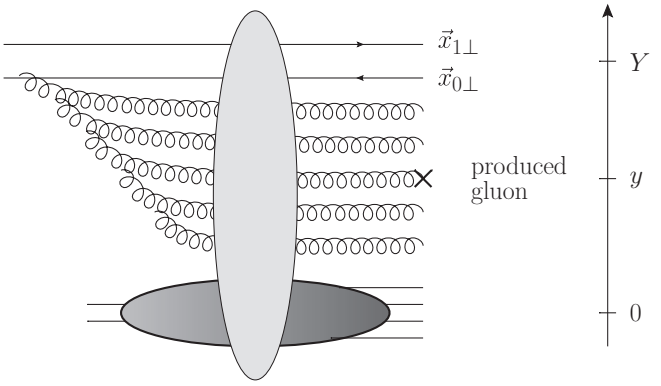

Fig. 8.9. Gluon production in dipole–nucleus scattering with small-x evolution emissions both between the produced gluon (marked by a cross) and the target nucleus and between the produced gluon and the projectile dipole.

assume that the target nucleus has zero rapidity and that the produced gluon has rapidity y. However, now the incoming projectile has rapidity Y such that there are large rapidity intervals between the projectile and the produced gluon and between the gluon and the target. The process is illustrated in Fig. 8.9 for the case of dipole–nucleus scattering: gluon emissions (and absorptions) are allowed everywhere in the rapidity interval from 0 to Y. The target nucleus may indeed break up in this inclusive process.

To include BK/JIMWLK evolution effects in the gluon production formula, let us consider the dipole–nucleus scattering case rather than the quark–nucleus scattering considered in the previous subsection. We start by generalizing Eq. (8.20) to the case of a dipole projectile (Kovchegov 2001):

$$\frac{d\sigma^{q\bar{q}A}}{d^2k_T dy}(\vec{x}_{10}) = \int d^2x_2\, d^2x_{2'}\, d^2x_1 e^{-i\vec{k}_\perp\cdot\vec{x}_{22'}} \frac{\alpha_s C_F}{4\pi^4} \sum_{i,j=0}^{1} (-1)^{i+j} \frac{\vec{x}_{2i}\cdot\vec{x}_{2'j}}{x_{2i}^2 x_{2'j}^2}$$
$$\times \left[N_G(\vec{x}_{i\perp}, \vec{x}_{2'\perp}, y) + N_G(\vec{x}_{2\perp}, \vec{x}_{j\perp}, y) \right.$$
$$\left. - N_G(\vec{x}_{2\perp}, \vec{x}_{2'\perp}, y) - N_G(\vec{x}_{i\perp}, \vec{x}_{j\perp}, y) \right], \tag{8.35}$$

where the quark in the dipole is located at $\vec{x}_{1\perp}$ and the antiquark is at $\vec{x}_{0\perp}$, as shown in Fig. 8.9. (The reader is invited to derive Eq. (8.35) in Exercise 8.2.)

Including the evolution in the rapidity interval between the gluon and the target is straightforward: in fact this was already done in deriving Eq. (8.20). Indeed, as we have seen above, the Wilson-line formalism used in arriving at (8.20) applies equally well to GGM multiple rescatterings and to the LLA evolution. We therefore conclude that N_G evaluated at rapidity y in Eq. (8.35) (and in Eq. (8.20) as well) does not need to come from multiple rescatterings only but may also contain the nonlinear BK/JIMWLK LLA evolution. In the large-N_c limit of BK evolution one can readily show that

$$N_G(\vec{x}_\perp, \vec{b}_\perp, y) = 2N(\vec{x}_\perp, \vec{b}_\perp, y) - N^2(\vec{x}_\perp, \vec{b}_\perp, y), \tag{8.36}$$

https://doi.org/10.1017/9781009291446.009 Published online by Cambridge University Press

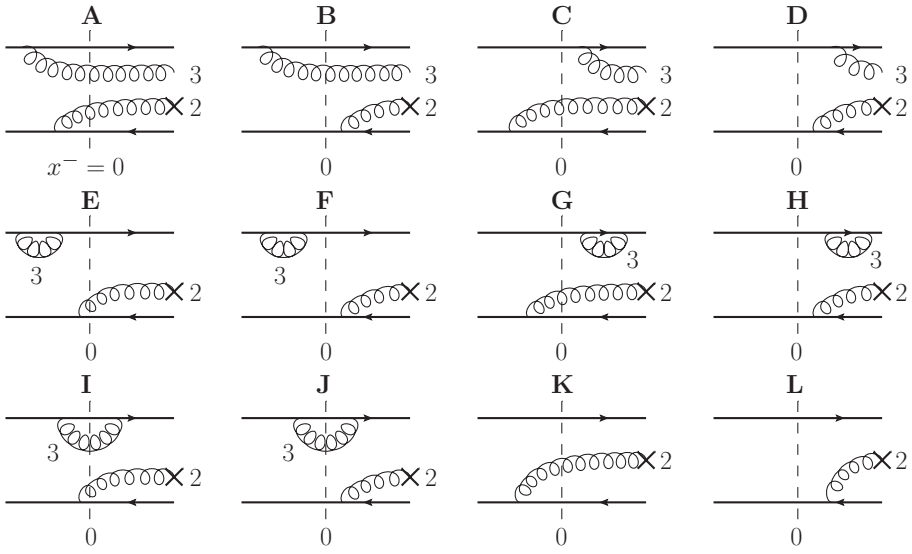

Fig. 8.10. One step of small-x evolution between the projectile onium and the produced gluon, marked by a cross and labeled 2.

where N is the quark dipole amplitude found from Eq. (4.138). The formula (8.36) is due to the fact that in the large-N_c a gluon dipole limit can be thought of as a pair of quark dipoles, with either one or both dipoles interacting directly with the target.

Including the evolution in the rapidity interval between the projectile and the produced gluon requires a bit more work. We will carry out the calculation in the large-N_c limit of Mueller's dipole model. We show one step of such an evolution in Fig. 8.10, where the gluon labeled 3 is harder than the produced gluon 2, that is $z_3 \gg z_2$ with z_2 and z_3 the fractions of the longitudinal momentum of the onium carried by the two gluons respectively. For simplicity we consider a case of particular couplings of the gluons to the onium: the gluon 3 is emitted (and absorbed) by the quark while gluon 2 is emitted by the antiquark. Diagrams A–D in Fig. 8.10 have two real emissions while in the diagrams E–J gluon 3 is virtual. For completeness, we show in diagrams K and L of Fig. 8.10 the emission of gluon 2 without the corrections due to gluon 3.

It is important to stress that we have only given the leading-logarithmic diagrams in Fig. 8.10. Indeed, a diagram similar to A but with the emission of gluon 2 before gluon 3 is possible but will not lead to leading logarithms of $1/x$ (see Fig. 4.17 and its evaluation for an analogous calculation). Similarly one can demonstrate that a diagram similar to D but with the emission of gluon 3 before gluon 2 also lies outside the LLA. This is an important observation: while for $x^- < 0$ the harder gluons are emitted before the softer ones, for $x^- > 0$ the harder gluons would need to be emitted *later* than the softer ones to give an LLA contribution. This rule is also valid for the virtual diagrams; this is illustrated by the fact that graph H in Fig. 8.10 gives an LLA contribution. (Indeed, we do not integrate over the rapidity y of gluon 2 since we are tagging this gluon (i.e., it is the

https://doi.org/10.1017/9781009291446.009 Published online by Cambridge University Press

gluon of interest): however, the leading contribution to the production cross section with all rapidity intervals large is given by the LLA approximation as if we were about to integrate over y.)

Using the cancellations of Fig. 7.10 (which are valid for the inelastic interactions with the target shown in Fig. 8.4 as well), one can write down the following relations between the squares and interference terms of the diagrams in Fig. 8.10:

$$|C|^2 + GK^* + G^*K = 0, \quad |D|^2 + HL^* + H^*L = 0, \tag{8.37a}$$

$$CD^* + GL^* + KH^* = 0, \qquad AC^* + IK^* = 0, \tag{8.37b}$$

$$BC^* + JK^* = 0, \quad AD^* + IL^* = 0, \quad BD^* + JL^* = 0. \tag{8.37c}$$

With the help of Eqs. (8.37) we see that

$$|A + B + \cdots + L|^2 \Big|_{O(\alpha_s^2)} = |A + B|^2 + (E + F)(K + L)^* + (E + F)^*(K + L), \tag{8.38}$$

that is, only emissions or absorptions of gluon 3 with $x^- < 0$ both in the amplitude and in the complex conjugate amplitude remain. This conclusion can be generalized to the case of other gluon couplings and, more importantly, to the case of higher-order hard gluon emissions: the terms which survive the cancellations of Fig. 7.10 are those with all the emissions and absorptions at $x^- < 0$ and $x'^- < 0$; all late-time ($x^-, x'^- > 0$) emissions cancel. We conclude that the evolution in the rapidity interval between the projectile and the produced gluon is the evolution of Mueller's dipole model! In fact an analysis of the higher-order diagrams shows that not all the nonlinear dipole evolution contributes: rather, the nonlinearities cancel leaving only the linear part of the evolution describing the generation by the original incoming onium of the dipole in which gluon 2 was emitted.[3] The quantity n_1 describing such a distribution is defined in Eq. (4.81) and is found from the dipole BFKL equation (4.82) with the initial condition (4.83).

We have thus arrived at the following physical picture of the gluon production process in DIS and pA at large N_c: the evolution in the projectile wave function generates a distribution of single dipoles. A gluon that we will tag (measure) is then emitted by one such dipole, making the evolution between the projectile and the produced gluon linear. The gluon along with the dipole from which it was emitted then interact with the target nonlinearly.

Formally the LLA evolution between the projectile and the produced gluon is included in Eq. (8.35) by the following replacement:

$$\frac{d\sigma^{q\bar{q}A}}{d^2k_T dy d^2B_\perp}(\vec{x}_{10}) \to \int d^2b_\perp d^2x_{1'0'}\, n_1(\vec{x}_{10}, \vec{x}_{1'0'}, \vec{B}_\perp - \vec{b}_\perp, Y - y) \times \frac{d\sigma^{q\bar{q}A}}{d^2k_T dy d^2b_\perp}(\vec{x}_{1'0'}), \tag{8.39}$$

[3] For instance, one can see that all subsequent evolution in the dipole formed by the (antiquark line of the) gluon 3 and the quark line in Fig. 8.10A cancels.

https://doi.org/10.1017/9781009291446.009 Published online by Cambridge University Press

where the impact parameters are labeled as in Fig. 8.6; $\vec{B}_\perp = (\vec{x}_{1\perp} + \vec{x}_{0\perp})/2$ is the center of the projectile dipole 10 and $\vec{b}_\perp = (\vec{x}_{1'\perp} + \vec{x}_{0'\perp})/2$ is the center of the dipole $1'0'$. Note that the integration over $\vec{b}_\perp$ for fixed $\vec{x}_{1'0'}$ in Eq. (8.39) is equivalent to the integration over $\vec{x}_{1\perp}$ in Eq. (8.35). Equation (8.35), which does not contain any evolution between the projectile and the produced gluon, is recovered from Eq. (8.39) by inserting Eq. (4.83) into it.

We can now write down the final expression for the gluon production in dipole–nucleus scattering. Combining Eq. (8.39) with Eq. (8.35) yields (Kovchegov and Tuchin 2002)

$$\begin{aligned}
&\frac{d\sigma^{q\bar{q}A}}{d^2k_T dy}(\vec{x}_{10}) \\
&\quad = \int d^2B_\perp d^2b_\perp d^2x_{1'0'}\, n_1(\vec{x}_{10}, \vec{x}_{1'0'}, \vec{B}_\perp - \vec{b}_\perp, Y - y) \\
&\qquad \times \int d^2x_2\, d^2x_{2'} e^{-i\vec{k}_\perp\cdot\vec{x}_{22'}} \frac{\alpha_s C_F}{4\pi^4} \sum_{i,j=0'}^{1'} (-1)^{i+j} \frac{\vec{x}_{2i}\cdot\vec{x}_{2'j}}{x_{2i}^2 x_{2'j}^2} \\
&\qquad \times \left[N_G(\vec{x}_{i\perp}, \vec{x}_{2'\perp}, y) + N_G(\vec{x}_{2\perp}, \vec{x}_{j\perp}, y) - N_G(\vec{x}_{2\perp}, \vec{x}_{2'\perp}, y) - N_G(\vec{x}_{i\perp}, \vec{x}_{j\perp}, y)\right].
\end{aligned} \tag{8.40}$$

This is the gluon production cross section including the LLA small-x evolution both between the projectile and the produced gluon and between the gluon and the target. While it has been derived in the large-N_c limit, Eq. (8.40) is also valid for any N_c as was shown by Kovner and Lublinsky (2006).

Equation (8.40) can also be written in a k_T-factorized form. Defining the unintegrated gluon distribution of the nucleus (cf. Eq. (8.28)) as

$$\phi_A(y, k_T^2) = \frac{C_F}{\alpha_s(2\pi)^3} \int d^2b_\perp d^2x_\perp e^{-i\vec{k}_\perp\cdot\vec{x}_\perp} \nabla_{\vec{x}_\perp}^2 N_G\left(\vec{x}_\perp, \vec{b}_\perp, y\right) \tag{8.41}$$

and that of the onium (cf. Eq. (8.4)) as

$$\begin{aligned}
\phi_{q\bar{q}}(y, k_T^2) = \frac{\alpha_s C_F}{\pi} \frac{1}{k_T^2} \int d^2b_\perp d^2x_\perp \left(2 - e^{-i\vec{k}_\perp\cdot\vec{x}_\perp} - e^{i\vec{k}_\perp\cdot\vec{x}_\perp}\right) \\
\times n_1\left(\vec{x}_{10}, \vec{x}_\perp, \vec{b}_\perp, y\right)
\end{aligned} \tag{8.42}$$

and evaluating Eq. (8.40) following steps similar to those in Sec. 8.2.1, we obtain (Braun 2000c, Kovchegov and Tuchin 2002)

$$\frac{d\sigma^{q\bar{q}A}}{d^2k_T\, dy} = \frac{2\alpha_s}{C_F} \frac{1}{k_T^2} \int d^2q_\perp\, \phi_{q\bar{q}}(Y - y, q_T^2)\, \phi_A\left(y, (\vec{k}_\perp - \vec{q}_\perp)^2\right). \tag{8.43}$$

We see that the LLA small-x evolution preserves the k_T-factorization of Eq. (8.30)!

https://doi.org/10.1017/9781009291446.009 Published online by Cambridge University Press

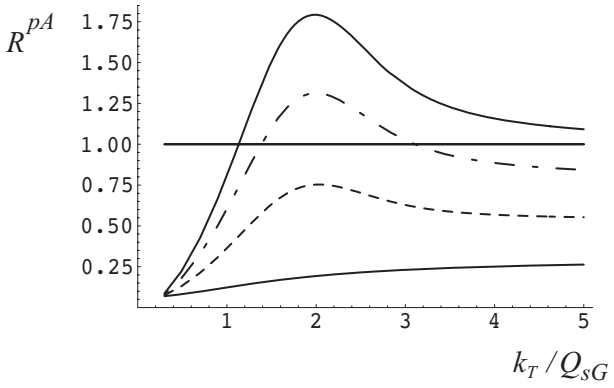

Fig. 8.11. A sketch of the nuclear modification factor as a function of k_T/Q_{sG}, where Q_{sG} is the typical saturation scale (see the caption to Fig. 8.8), for gluon production in pA collisions: the upper solid line corresponds to the quasi-classical approximation from Fig. 8.8, while the dashed-and-dotted, dashed, and lower solid lines demonstrate the change in R^{pA} with increasing rapidity, owing to small-x evolution. (Reprinted with permission from Kharzeev, Kovchegov, and Tuchin (2003). Copyright 2003 by the American Physical Society.)

Equation (8.43) can be generalized to the case of any projectile, in particular the proton, for which we define the unintegrated gluon distribution

$$\phi_p(y, k_T^2) = \frac{C_F}{\alpha_s (2\pi)^3} \int d^2 b_\perp d^2 x_\perp e^{-i\vec{k}_\perp \cdot \vec{x}_\perp} \nabla^2_{\vec{x}_\perp} n_G(\vec{x}_\perp, \vec{b}_\perp, y), \tag{8.44}$$

with n_G the gluon dipole–proton forward scattering amplitude evolved by the linear BFKL evolution equation. One then writes for the inclusive gluon production cross section (Braun 2000c, Kharzeev, Kovchegov, and Tuchin 2003)

$$\frac{d\sigma^{pA}}{d^2 k_T \, dy} = \frac{2\alpha_s}{C_F} \frac{1}{k_T^2} \int d^2 q_\perp \, \phi_p(Y - y, q_T^2) \, \phi_A \left(y, (\vec{k}_\perp - \vec{q}_\perp)^2 \right). \tag{8.45}$$

The gluon spectrum generated by Eq. (8.45) is qualitatively similar to that obtained in the quasi-classical approximation in Fig. 8.7: the IR divergence is softened to $1/k_T^2$, though it is not removed completely. The nuclear modification factor R^{pA} resulting from using Eq. (8.45) is very different from the quasi-classical one in Fig. 8.8 and is shown in Fig. 8.11; the various curves correspond to different values of rapidity y, such that the lower the curve the higher is the rapidity y. The effect of small-x evolution and saturation is such that the quasi-classical Cronin enhancement at large k_T is replaced by suppression at all values of k_T (Kharzeev, Levin, and McLerran 2003, Albacete *et al.* 2004, Kharzeev, Kovchegov, and Tuchin 2003). The diagram in Fig. 8.11 was confirmed by the precise numerical evaluation of R^{pA} by Albacete *et al.* (2004).

To understand this result analytically we use the approximate solution of the fixed-coupling BK equation immediately outside the saturation region given by Eq. (4.161). Concentrating on its A-dependence we see that $N_G \sim A^{(1+2i\nu_0)/6}$, where we employ the

https://doi.org/10.1017/9781009291446.009 Published online by Cambridge University Press

facts that $N_G \sim N$ in this linear-evolution region (see Eq. (8.36)) and that $Q_{s0} \sim A^{1/6}$. Using this in Eq. (8.41) we see that $\phi_A \sim S_\perp A^{(1+2i\nu_0)/6} \sim A^{5/6+i\nu_0/3}$. This factor is the only source of A-dependence in Eq. (8.45). Using the latter in Eq. (8.33) we obtain (Kharzeev, Levin, and McLerran 2003)

$$R^{pA}(k_T \gtrsim Q_{sG}) \sim A^{-1/6+i\nu_0/3} = A^{-0.124} \ll 1 \qquad \text{for } A \gg 1. \tag{8.46}$$

We see that for large enough nuclei and for large rapidities y (such that Eq. (4.161) is applicable) the nuclear modification factor in pA collisions becomes smaller than 1, in agreement with Fig. 8.11.

8.3 Gluon production in nucleus–nucleus collisions

An important problem, both from the standpoint of saturation physics and for the physics of ultrarelativistic heavy ion collisions, is to find the gluon production cross section for nucleus–nucleus (AA) collisions. Practically, the problem means that one has to find the gluon transverse momentum spectrum in the case when neither the saturation scale of the projectile Q_{s1} nor the saturation scale of the target Q_{s2} is negligibly small in the k_T-range of interest. The solution of the problem would involve first constructing a quasi-classical solution for the MV model with multiple rescatterings in both colliding nuclei. On top of that one would have to include quantum small-x evolution. Phenomenological applications would also require fixing the scales of all the coupling constants in the expression.

At the time of writing none of the above steps has been done analytically. For some theoretical developments see Balitsky (2004), Blaizot and Mehtar-Tani (2009), and Kovchegov (2001). One may perhaps expect that the persistence of the k_T-factorization formula (8.45) for various approximations of gluon production in pA and DIS would indicate that this formula could be valid for AA collisions as well. However, in AA collisions both nuclei come in with fully saturated wave functions, which are completely screened in the IR (see Eq. (5.56) and Fig. 5.7): one would therefore expect that owing to the lack of low-k_T partons the produced-gluon spectrum would have no power-law divergence at small k_T, making it unlikely that k_T-factorization gives the right answer for gluon production in AA collisions. To see this, note that, an inspection of Eq. (8.45) shows that it always leads to $1/k_T^2$ divergence at small k_T, thus contradicting the physical argument we have just presented. Furthermore, the k_T-factorization formula does not appear to agree with the results of numerical solutions of the quasi-classical AA problem.

The quasi-classical gluon field in AA collision was found numerically in the works of Krasnitz and Venugopalan (2000, 2001), Lappi (2003), and Krasnitz, Nara, and Venugopalan (2003a, b). In Fig. 8.12 we show the resulting gluon spectrum and, for comparison, the predictions of the k_T-factorization formula (8.30) (Blaizot, Lappi, and Mehtar-Tani 2010). The solid line in Fig. 8.12 gives the gluon spectrum multiplied by k_T^2 as a function of k_T/Q_{sG} for a numerical solution of the classical Yang–Mills equations with the two nuclei giving the source current ($Q_{sG} = 2$ GeV; the IR cutoff $\Lambda = 0.1$ GeV). The prediction of the k_T-factorization formula (8.30) is shown by the dotted line in Fig. 8.12: one can clearly see that while the two curves are close to each other for $k_T \gtrsim Q_{sG}$, Eq. (8.30) deviates from

https://doi.org/10.1017/9781009291446.009 Published online by Cambridge University Press

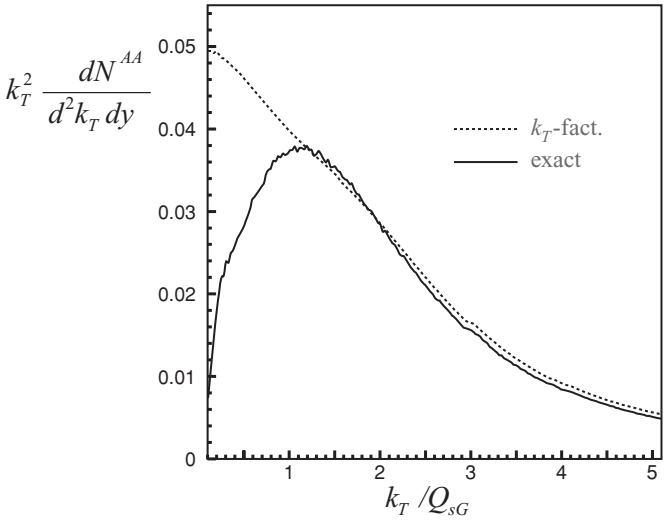

Fig. 8.12. The gluon spectrum multiplied by k_T^2 in AA collisions in the quasi-classical approximation as a function of k_T/Q_{sG}, given by a numerical solution (solid line). The dotted line represents the prediction of the k_T-factorization formula (8.30). (Reprinted from Blaizot, Lappi, and Mehtar-Tani (2010), with permission from Elsevier.) A color version of this figure is available online at www.cambridge.org/9780521112574.

the full solution for $k_T \lesssim Q_{sG}$. In fact $k_T^2 dN^{AA}/d^2k_T dy$ for the full numerical solution goes to zero as $k_T \to 0$, so that the total multiplicity dN^{AA}/dy is independent of the IR cutoff, in agreement with the physical argument presented above.

A promising strategy for including small-x evolution corrections in numerical simulations of the quasi-classical gluon production was proposed recently by Gelis, Lappi, and Venugopalan (2007, 2008a, b, 2009). It involves a new type of k_T-factorization in which the JIMWLK evolutions of both nuclei factorize, each providing sources for quasi-classical gluon production.

Further reading

In this chapter we presented theoretical developments addressing single inclusive gluon production in high energy collisions in the saturation/CGC framework. The techniques presented here have been used to calculate other inclusive observables in DIS and pA collisions. Single inclusive valence quark production was found by Dumitru and Jalilian-Marian (2002) for a hard quark, while the valence quark production at mid-rapidity was calculated by Albacete and Kovchegov (2007a). The prompt photon production cross section was derived by Gelis and Jalilian-Marian (2002a). Two-particle inclusive production (and hence particle correlations) can also be determined. Di-lepton pair production (the Drell–Yan process) was found by Gelis and Jalilian-Marian (2002b), Baier, Mueller, and Schiff

https://doi.org/10.1017/9781009291446.009 Published online by Cambridge University Press

(2004), and Kopeliovich *et al.* (2003). Inclusive two-gluon production was found by Jalilian-Marian and Kovchegov (2004) and by Kovner and Lublinsky (2006). Gluon–valence-quark production was calculated by Marquet (2007) and, using a different technique, by Jalilian-Marian and Kovchegov (2004). Quark–antiquark pair production was found by Blaizot, Gelis, and Venugopalan (2004) and by Kovchegov and Tuchin (2006). A number of properties of two-particle correlations have been discussed recently by Dominguez *et al.* (2011).

Exercises

8.1 Show that the lowest-order gluon production in onium–onium scattering is given by Eq. (8.3) with the unintegrated gluon distributions given by Eq. (8.4).

8.2 Show that the inclusive gluon production cross section in onium–nucleus scattering and in the quasi-classical MV/GGM approximation is given by Eq. (8.35). Demonstrate that this expression can be reduced to the k_T-factorized form (8.30).

8.3 Using a simplified model for N_G,

$$N_G(\vec{x}_\perp, \vec{b}_\perp, 0) = 1 - \exp\left\{-\frac{x_\perp^2 Q_{sG}^2}{4}\right\}, \tag{8.47}$$

and assuming that Q_{sG}^2 is $\vec{b}_\perp$-independent in a very large circle of radius R and is zero outside the circle, evaluate Eq. (8.20) exactly. Use the obtained expression to construct the nuclear modification factor R^{pA} defined in Eq. (8.33). Plot the resulting R^{pA} as a function of k_T/Q_{sG} and compare the plot with Fig. 8.8.

8.4 Prove the cancellations in Eqs. (8.37).

8.5* Reduce Eq. (8.40) to Eq. (8.43) using the unintegrated gluon distributions defined in Eqs. (8.41) and (8.42).

https://doi.org/10.1017/9781009291446.009 Published online by Cambridge University Press